20

InAs Infrared Photodiodes

Volodymyr Tetyorkin[1], Andriy Sukach[1] and Andriy Tkachuk[2]
[1]*V. Lashkaryov Institute of Semiconductor Physics NAS of Ukraine*
[2]*V.Vinnichenko Kirovohrad State Pedagogical University*
Ukraine

1. Introduction

The performance of infrared InAs homojunction and heterojunction photodiodes (PDs) and possibilities of its improvement are analyzed both theoretically and experimentally. The PDs are diffusion-limited at room temperature. An excess current at low temperatures is analyzed within a model of non-homogeneous p-n junction. The excess current is shown to be caused by tunneling of carriers via deep defect states in the gap. The carrier lifetime in InAs is calculated for radiative and Auger recombination mechanisms using three- and four-band Kane models. Theoretical limits of threshold parameters in homojunction and heterojunction PDs are calculated. Experimentally proved that p^+-InAsSbP/n-InAs heterojunction PDs can be more effective as sensitive element in gas sensors operated at room temperature in comparison with commercially available PDs. They have more broad spectral response and higher values of the resistance-area product at zero bias voltage.

2. Current status of InAs photodiodes

Mid-wavelength infrared (MWIR) photodetectors, light-emitting diodes (LEDs) and lasers are important components of modern infrared optoelectronic sensors. Despite the fact that MWIR region can be covered by different IV-VI and II-VI photodetectors (e.g., PbS and PbSe photoconductors, HgCdTe photodiodes and photoconductors, InAs PDs are expected to be the best choice from both practical and economic point of view due to mature technology of low-cost InAs substrates. The main advantage of InAs PDs is that they can operate at room and near room temperatures. The elimination of cryogenic cooling system results in significant reduction in cost and more reliable operation of infrared devices on their base. InAs PDs exhibit better noise characteristics at low frequencies and offer superior pulse response for detecting rapid processes in comparison with IV-VI photoconductors. Their characteristics (sensitivity, differential resistance, peak wavelength) can be optimized for specific purposes. The important fact is that InAs and ternary compounds on its base are also used for manufacture of LEDs (Zotova, 1991; Popov,1997; Matveev, 2002). The emission and photoresponse spectra of LEDs and PDs can be easily matched at different temperatures. In comparison with II-VI and IV-VI IR detectors, InAs PDs exhibit more stable characteristics. Commercially available InAs PDs are produced by Judson Technologies LLC and Hamamatsu Corporation as single-element structures. Apparently, the multielement structures exist only as laboratory samples. InAs infrared PDs have different applications such as conventional and laser spectroscopy, gas analysis, thermal imaging, remote sensing.

At the same time these PDs are characterized by rather low values of the differential resistance - area product R_0A at room temperature. This seems to be the main reason that InAs infrared photodetectors operate in sub-BLIP regime (Rogalsky, 1995). Further improvement in their performance is possible with a decrease in dark current and supression of Auger recombination.

3. Preparation of photodiodes and experimental techniques

Homojunction PDs were prepared by short-term (20-30 min) diffusion of Cd into n-InAs substrates at T=875 K. The substrates of n-type conductivity were cut from single-crystal ingots grown in joint-stock company "Pure metals plant" (Svetlovodsk, Ukraine). The damaged surface layers were removed by using dynamic chemical-mechanical polishing in 2% Br_2–CH_3OH solution. Their structural quality was controlled by X-ray diffraction method. In the chemically polished substrates the rocking curves half-width was 25-27″. Electrical parameters were controlled by van der Pauw technique at 295 K. The carrier concentration and mobility were found to be $n=(2\div3)\times10^{16}$ cm^{-3} and $\mu_n=(2\div2.5)\times10^4$ $cm^2/V\times s$, respectively. The density of dislocations was in the range $(2\div4)\times10^4$ cm^2. The substrates with the diffused p-type layer had mirror-like surfaces free of structural damages such as inclusions of impurity atoms. They were characterized by the rocking curve half-width of 32-35″. Typical profiles of Cd atoms in a substrate are shown in Fig.1. As seen, at low values of depth x they can be approximated by two exponential dependences (shown by solid lines in Fig. 1). Similar profiles of impurity atoms were previously observed in GaAs (Grigor'ev & Kudykina, 1997) and explained by generation of non-equilibrium vacancies at the substrate's surface. In such a case, an impyrity profile is determined by distribution of vacancies under the surface. The junction depth was determined from the probe thermo-emf measurements during careful chemical etching of diffused layers. Mesa structures were prepared on (111)A side of substrates by chemical etching in 2% Br_2-HBr solution. In order to eleiminate the surface leakage current mesas were passivated by etching in HNO_3-based solution followed by deposition of anode oxide doped with fluorine with thickness of 0.3 μm. After passivation they were covered by thin layer of ZnTe thermally deposited in a vacuum chamber at temperature 150 ^oC.

The heterojunction p^+-InAsSbP/n-InAs PDs were prepared by LPE technique in IOFFE Physico-Technical Institute, St.-Petersbur Russia (Zotova, 1991; Matveev, 1997; Matveev, 2002). For this purpose, lattice matched InAsSbP epitaxial layers of approximately 3 μm thickness were grown on (111)B surfaces of InAs substrates. The quaternary InAsSbP compound had energy gap of 0.43 eV at T = 297 K. The epilayers were doped to about 10^{18} cm^{-3} by addition of Zn to the melt. The substrates were n-type single crystals with electron concentration $n=(2\div3)\times10^{16}$ cm^{-3}. In homojunction and heterojunction PDs mesa structures have active area $A=4x10^{-2}$ cm^{-2} and 1.45×10^{-3} cm^2, respectively.

In order to characterize the prepared PDs, the dark current as well as the high-frequency (1 MHz) barrier capacitance were measured as a function of bias voltage and temperature. The carrier lifetime was determined from the photoconductivity signal decrease recorded by a memory oscilloscope in the temperature range 77-300 K. The investigated samples were illuminated by Nd:YAG pulsed laser with the pulse width around 2 ns. It has been observed that the signal decrease was not exactly exponential: a very fast decrease was observed immediately after the end of illumination followed by an exponential slow decrease. The excess carrier lifetime was associated with the slow decrease. The fast decrease, not typical

for recombination processes, was associated with a high-level excitation of excess carriers. The photoresponse spectra were measured in the short-circuit current mode using grating monochromator and halogen lamp as a source of light. The photoresponse signal was recorded by a lock-in amplifier and processed by a personal computer.

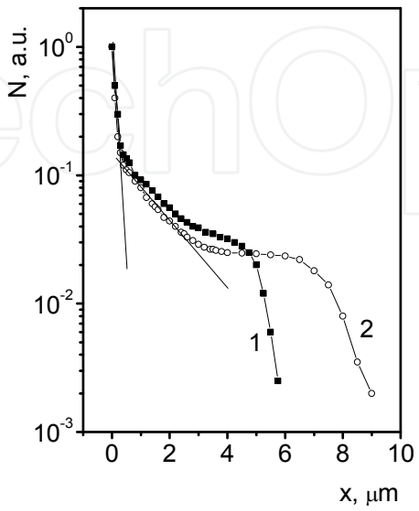

Fig. 1. SIMS profiles of Cd in InAs. The diffusion time is 20 min (1) and 30 min (2).

4. Recombination mechanisms in InAs

The carrier lifetime in narrow-gap semiconductors is determined by a number of recombination mechanisms, such as radiative, Auger and Shockley-Read-Hall recombination. The theory of radiative recombination has been developed by Van Roosbroeck and Shockley (Van Roosbroeck & Shockley, 1959; Blakemore, 1962). Ten types of possible band-to-band Auger recombination processes in n- and p-type semiconductors were determined by Beattie (Beattie, 1962). The Auger 1 recombination mechanism in n-type material with InSb-like band structure was firstly considered by Beattie and Landsberg (Beattie & Landsberg, 1959). The Auger 7 process is important in p-type material if the split-off band can be ignored (Beattie & Smith, 1967; Takeshima, 1972). The role of the split-off band in InAs was firstly recognized by Takeshima (Takeshima, 1972). Since the split-off energy Δ in InAs is close to the energy gap E_g, the Auger S process may be dominant in p-type material. Further investigations of recombination processes in InAs were based on these pioneering works (Blakemore, 1962; Rogalski, 1995).

Three types of Auger recombination mechanisms (Auger 1, Auger 7 and Auger S) have been shown to be important in InAs (Takeshima,1972; Takeshima, 1975; Rogalski. & Orman, 1985). According to Rogalski and Orman, contributions of Auger and radiative mechanism are comparable at room temperatures in samples with the carrier concentration of the order of 10^{16} cm^{-3}. The Auger lifetime was theretically analyzed by Barishev (Barishev, 1964). The well known problem connected with the Auger recombination processes is the uncertainty introduced by the overlap integrals F_1 and F_2. For instance, in n-type InAs the value of $|F_1F_2|^2$ is ranged within an order of magnitude. Appropriate analysis in p-type materials is

even more difficult because of experimental data are rather scarce. An improvement in the calculation of overlap integrals was done by Gelmont with co-authors. The Auger S and Auger 7 processes were reexamined for the three- and four-band Kane models of band structure (Gelmont, 1978; Gelmont, 1981; Gelmont, 1982; Gelmont & Sokolova, 1982). The SRH recombination process in InAs is investigated unsufficiently. On the other hand, frequently observed large scattering of experimental data in samples with close values of free cariers density clearly specifies an essential role of this process.
The lifetime in InAs was calculated as a fuction of temperature and density of carriers. The calculated lifetime is compared with experimental data available in the literature (Datal, 1979; Wider & Collins, 1974; Andrushko, 1986; Fomin, 1984; Blaut-Blachev, 1975; Bolgov, 1997). For small departure from equilibrium the radiative lifetime is given by

$$\tau_R = \frac{1}{B(n_o+p_o)} \tag{1}$$

where n_o and p_o are the equilibrium electron and hole concentrations. The capture probability B for parabolic conduction and valence bands is given by

$$B = 5.8\times 10^{-13}\varepsilon_\infty^{1/2}\left(\frac{m}{m_e^*+m_h^*}\right)^{3/2}\left(1+\frac{m_o}{m_e^*}+\frac{m_o}{m_h^*}\right)\left(\frac{300}{T}\right)^{3/2}E_g^2 \tag{2}$$

where ε_∞ is the high-frequency dielectric constant, m_e^* and m_h^* are the effective masses of electrons and holes, respectively, the energy gap E_g is expressed in eV (Rogalski & Orman, 1985). For n-type material the Auger 1 recombination lifetime is equal to (Rogalski, 1995; Rogalski & Orman, 1985)

$$\tau_{A1} = \frac{n_i^2}{n(n_o+p_o)g_{A1}} = \frac{2n_i^2\tau_A^i}{n_o(n_o+p_o)} \tag{3}$$

where τ_A^i is the carrier lifetime in the intrinsic material. The Auger 7 lifetime in the limit of small excitation is equal to

$$\tau_{A7} = \frac{2\tau_{A7}^i}{1+p_o/n_o} \tag{4}$$

where

$$\tau_{A7}^i = \frac{p_0}{2g_{A7}^G} \tag{5}$$

Analogous equations for the carrier lifetime can be written for the Auger S process. The effective carrier lifetime is given by

$$\frac{1}{\tau} = \sum_i \frac{1}{\tau_i} \tag{6}$$

where τ_i is the carrier lifetime determined by the *i*th recombination process. The generation rate for the Auger 1 process g_{A1} obtained by Beattie and Landsberg is given by

$$g_{A1} = \frac{8(2\pi)^{5/2} e^4 m_e^* |F_1 F_2|^2 n_o}{h^3 \varepsilon^2 (1+\mu)^{1/2}(1+2\mu)} \left(\frac{kT}{E_g}\right)^{3/2} \exp\left[-\left(\frac{1+2\mu}{1+\mu}\right)\frac{E_g}{kT}\right] \quad (7)$$

According to Gelmont, in the three-band Kane model the generation rate is given by

$$g_{A1}^G = 3\left(\frac{2}{\pi}\right)^{1/2} \frac{e^4 m_e^* n_o}{\hbar^3 \varepsilon^2} \left(\frac{kT}{E_g}\right)^{5/2} \exp\left[-(1+2\mu)\frac{E_g}{kT}\right] \quad (8)$$

For the Auger 7 lifetime the generation rate is

$$g_{A7}^G = \frac{18 m_o (m_{hh}^*/m_o) e^4}{\pi \hbar^3 \varepsilon^2} p_o \left(\frac{kT}{E_g}\right)^{7/2} \exp\left[-(1+\frac{m_{hl}^*}{m_{hh}^*})\frac{E_g}{kT}\right] g(\alpha) \quad (9)$$

In the last three expressions, ε is the static dielectric constant, m_{hl}^* and m_{hh}^* are the effective masses of light and havy holes, respectively, μ is the ratio of the electron to the heavy-hole effective mass. The generation rate in the Auger S process depends on difference between the split-off and band gap energies. The most frequently used expressions for these energies are as follows (Rogalski. & Orman, 1985, Madelung, 1964):

$$E_g = 0.44 - 2.8\times10^{-4} T \quad (10)$$

and

$$\Delta = 0.43 - 1\times10^{-4} T \quad (11)$$

Since in the temperature range 77 – 300 K the condition $\Delta > E_g$ is fulfilled, the generation rate is given by (Gelmont, et al., 1982)

$$g_{AS}^G = \frac{27}{5}\pi^4 n_i^2 p_o \frac{e^4 \hbar^3 (m_s^*)^{5/2}(\Delta - E_g)\exp[-(\Delta - E_g)/kT]}{\varepsilon^2 (m_{hh}^*)^3 (m_e^*)^{3/2} kT \Delta^2 (E_g + \Delta)} \quad (12)$$

where m_S^* is the effective mass of holes in the split-off band, n_i is the intrinsic concentration. The concentration dependences of the carrier lifetime in n-type InAs are shown in Fig.2 and 3. At low temperature T=77 K experimental data are well described by the radiative recombination mechanism. The contribution of the Auger 1 recombination increases with an increase in temperature. The pronounced scattering of experimental data at room temperature may be caused by contribution of any SRH recombination process at high temperatures to the measured lifetime.

Experimental and calculated dependences for *p*-InAs are shown in Fig.4 and 5.

Three recombination mechanisms radiative, Auger 7 and Auger S were taken into account. The main result of theoretical calculations is as follows: the Auger 7 process is dominant recombination process in p-InAs. The contribution of the radiative mechanism is essential at a concentration of holes around 10^{16} cm^{-3}. The Auger S recombination mechanism is weakly dependent on temperature and its contribution to the lifetime is less important. Since the

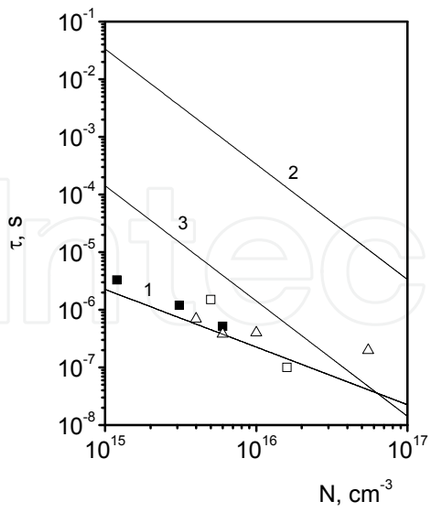

Fig. 2. Carrier lifetime vs doping level in *n*-InAs at 77 K (Tetyorkin, 2007). Solid curves are calculated for recombinations: 1 - radiative, 2 - Auger 1 (Gelmont), 3 – Auger 1 (Beattie and Landsberg, $|F_1F_2|^2$ equals 0.079).

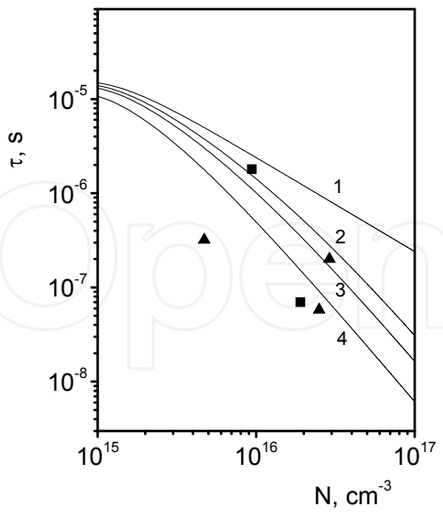

Fig. 3. Carrier lifetime vs doping level in *n*-InAs at 300 K (Tetyorkin, 2007). Calculated curves are obtained for: 1- radiative lifetime, 2 - radiative and Auger 1 (Gelmont), 3,4 -radiative and Auger 1 (Beattie and Landsberg, $|F_1F_2|^2$ equals 0.014 and 0.079, respectively).

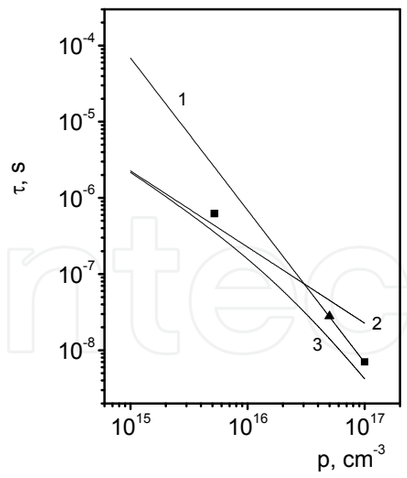

Fig. 4. Carrier lifetime vs. hole concentration at T=77 K (Tetyorkin, 2007). Calculated curves represent Auger 7 (1), radiative (2) and effective (3) lifetime which includes radiative, Auger 7 and Auger S recombinations.

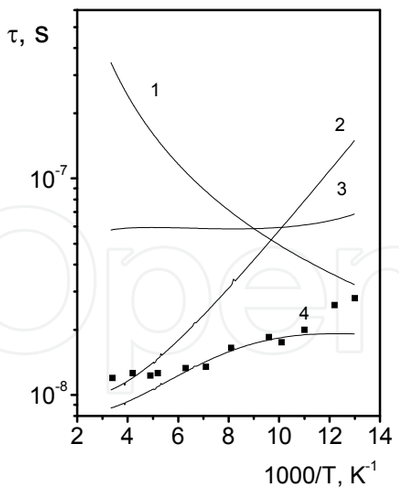

Fig. 5. Carrier lifetime vs temperature in *p*-InAs with $p=5\times10^{16}$ cm^{-3} (Tetyorkin, 2007). Calculated curves represent radiative (1), Auger 7 (2), Auger S (3) and effective (4) lifetime.

lifetime calculated for the Auger S mechanism is strongly dependent on the difference between Δ and E_g, this conclusion is based on values which were most often published in the literature.
Careful analysis of experimental values of the carrier lifetime obtained from the early 1960s to our days clearly indicate tendecy to their decrease. Gradually they have reaches theoretical limit which is determined by the radiative and Auger recombination processes. Obviously, this result is caused by improvements in technology of InAs single crystalls. On the other hand, the SRH recombination process still remains unsufficiently investigated. The role played by deep defects in the carrier transport mechanisms in PDs is analysed below.

5. Carrier transport mechanisms

The carrier transport mechanisms were analysed within one-dimensial analytic model. This model includes current from quasineutral and depletion regions of the junction (diffusion and generation-recombination currents), trap-assisted and band-to-band tunneling across the junction. In the investigated PDs the leakage current was treated as a bulk phenomenon.
The diffuson and generation current density was calculated by using the formulas:

$$I_D = qn_i^2\left(\frac{1}{p}\sqrt{\frac{D_n}{\tau_n}} + \frac{1}{n}\sqrt{\frac{D_p}{\tau_p}}\right) \tag{13}$$

and

$$I_{GR} = \frac{qn_i W}{2\tau_o} \tag{14}$$

where W is the depletion region width, τ_0 is the effective lifetime in the depletion region, D_n, τ_n and D_p, τ_p are the diffusion coefficient and the carrier lifetime for electrons and holes, respectively. As a rule, the effective lifetime served as adjusting parameter in calculations.
The band-to-band tunneling current density was calculated for the triangular barrier model (Sze, 1981).

$$I_{BTB} = \frac{\sqrt{2m_e^*}q^3FU}{4\pi^2\hbar^2E_g^{1/2}}\exp\left[-\frac{4\sqrt{2m_e^*}E_g^{3/2}}{3q\hbar F}\right] \tag{15}$$

where F is the electric field in the junction.
The trap-assisted tunneling current in InAs photodiodes was firstly investigated by A. Sukach and V. Tetyorkin (Sukach, 2005; Tetyorkin, 2005). For this purpose, a model of the trap-assisted tunneling developed earlier for HgCdTe photodiodes (Nemirovsky & Unikovsky, 1992; Rosenfeld & Bahir, 1992) was used. This model is based on number of simplifying assumptions, namely: shallow impurities and traps are uniformly distributed in the depletion region; the electric field across the depletion region is constant; transitions of electrons and holes occure via single level in the gap; initial states are occupied and final states are empty; in degenerate diodes the Burstein-Moss shift results in higher potential barriers for thermal and tunnel transitions of cariers. Traps can exchange carriers with the valence and conduction bands by tunnel and thermal transitions. Under these assumptions, the rates of tunneling transitions between the allowed bands and a trap in the gap is given by

$$\omega_v N_v = \frac{\pi^2 q m_h^* F M^2}{h^3 (E_g - E_t)} \exp\left[-\frac{4\sqrt{2m_h^*}(E_g - E_t)^{3/2}}{3q\hbar F} \right] \tag{16}$$

and

$$\omega_c N_c = \frac{\pi^2 q m_e^* F M^2}{h^3 E_t} \exp\left[-\frac{4\sqrt{2m_e^*} E_t^{3/2}}{3q\hbar F} \right] \tag{17}$$

where the trap energy E_t is measured from the edge of the conduction band. The matrix element M between the trap wave function and the conduction band Bloch wave function in silicon is of the order of 10^{-29} $(eV)^2 cm^3$ (Rosenfeld & Bahir, 1992). Its value can be also estimated by using the formula (Wenmu He & Zeynep Celik-Batler, 1996).

$$M = \frac{2\hbar^2\sqrt{2\pi}}{m_o}\left(\frac{2m_o}{\hbar^2}\right)^{1/4} \frac{E_g}{E_t^{3/4}} \tag{18}$$

Then the trap-assisted tunneling current is given by

$$J_{tat} = qWN_t\left(\frac{1}{\omega_v N_v + c_p p_1} + \frac{1}{\omega_c N_c + c_n n_1}\right)^{-1} \tag{19}$$

where $c_p p_1$ and $c_n n_1$ are the rates of thermal transitions. The concentration of traps N_t, trap energy E_t and capture cross section for electrons and holes c_n and c_p are obtained from the fitting calculations.

Typical forward and reverse I-U characteristics of a representative diffused PD are shown in Fig.6 and 7. It is necessary to note presense of two exponential regions at temperatures T ≤ 180 K, Fig. 6. The slope of the first region measured at lower biase voltages increases with temperature increasing. The second region exhibits an opposite dependence of the slope on temperature. At higher temperatures the only exponential region is obseved.

For analysis of carrier transport mechanisms in diffused PDs, the current-voltage characteristics should be corrected to the series resistance R_s. This correction is especially important due to possible formation of high-resistance compensated region. The presence of this region has been proved with capacitance-voltage measurements shown in Fig. 8.

The following peculiarities should be pointred out: experimental curves are linearized in coordinates typical for abrupt p-n junctions; the slope of C^{-2}-U dependences is weak function of temperature; the concentration of free carriers determined from their slope is ranged from 1.5×10^{15} at 77 K to 3.0×10^{15} cm^{-3} at 295 K. These values are approximately one order of magnitude lower than the carrier concentration in the starting material. The high-resistance compensated region results in the capacitance saturation at forward biase voltages. The width of the compensated region, estimated from this saturation, was in the range 2.5 - 3 μm. Since these values substantially exceed the depletion region width (W≈0.6 μm at zero bias voltage), the p-n junction is presumably located inside the compensated region. It has been assumed that the diffused PDs have p^+-p_o-n_o–n junction structure. Experimental I-U characteristics were approximated by exponential dependence

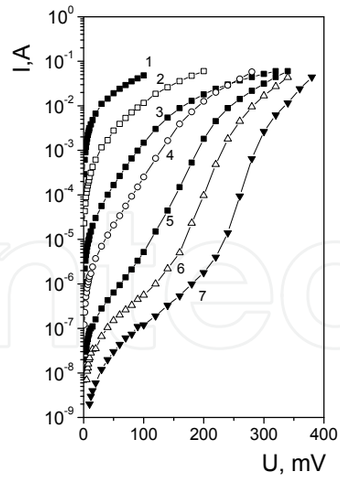

Fig. 6. Forward I-U characteristics in a diffused PD at temperatures, K: 1- 290, 2 – 255, 3 – 218, 4 – 197, 5 – 158, 6 – 135, 7 – 77. (Sukach, 2005).

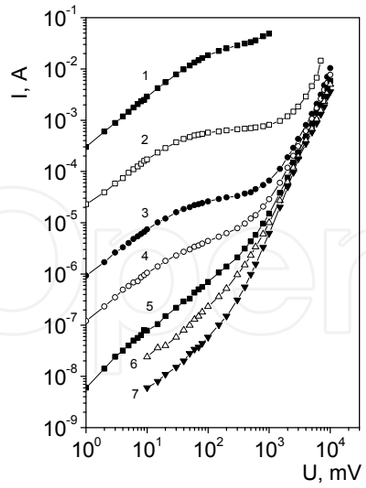

Fig. 7. Reverse current-voltage characteristics measured at the same temperatures as in Fig.6. (Sukach, 2005).

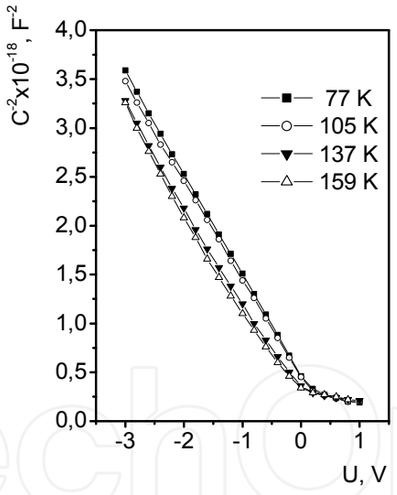

Fig. 8. Capacitance-voltage characteristics in a diffused photodiode at different temperatures (Sukach, 2005).

$$I = I_O\left\{\exp[(qU - IR_S)/\beta kT] - 1\right\} \tag{20}$$

The ideality coefficient extracted from the slope of R_s-corrected I-U curves is ranged from 5.9 to 1.1 and from 1.6 to 1.1 for the first and second exponential regions in Fig. 6, respectively. The reverse current saturation is observed only at high temperatures for narrow interval of biase voltages. At low temperatures the current-voltage characteristics have a form typical for the soft breakdown.

In the diffusion-limited diode the ideality coefficient β = 1. So, experimental data shown in Fig.6 and 7 clearly indicate presence of additional currents in the investigated PDs. Based on experimental values of the ideality coefficient, one can conclude that the diffusion current is dominant at room temperature. Predominance of diffusion and generation currents at reverse biase voltages was confirmed by theoretical calculations within the model of symmetrical p^+-p_o-n_o–n junction, Fig.9. As seen, the contribution of the generation current is increased with the reverse bias increasing, Fig.9.

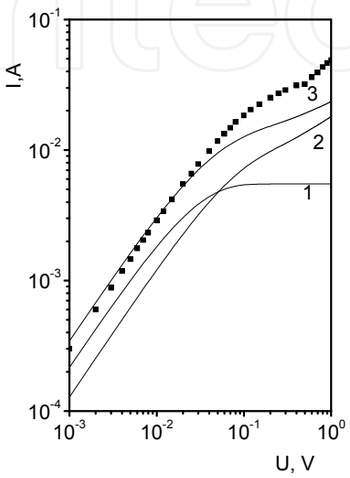

Fig. 9. Measured (dots) and calculated (solid lines) reverse current-voltage characteristics of a diffused PD at 290 K. Calculated curves represent diffusion (1), generation (2) and total (3) current. Parameters used for calculation: $\tau_o = 1.5\times10^{-9}$ s, $n_i = 5.6\times10^{14}$ cm^{-3}, $\tau_n = \tau_p = 1\times10^{-9}$ s, $n_o = p_o = 3\times10^{15}$ cm^{-3}, $\mu_n = 10^3$ cm^2/V×s, $\mu_p = 150$ cm^2/V×s, $U_D = 110$ mV (Sukach, 2005).

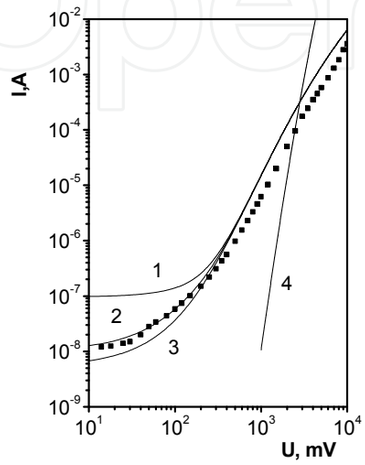

Fig. 10. Calculated (1-3) trap-assisted tunneling current (see text) in a model of nonhomogeneous p-n junction. Curve 4 represents the band-to-band tunneling current (Sukach, 2005). Experimental data are obtained for a diffused PD.

Large values of the ideality coefficient at low temperatures most probably indicate that the additional current is tunneling. To prove this assumption, band-to-band and trap-assisted tunneling currents were calculated using the above formulas. In order to reduce possible uncertainties in theoretical calculations caused by large amount of unknown adjusting parameters, the trap-assisted tunneling current was calculated for the midgap traps. Such traps with density 10^{13} – 10^{14} cm^{-3} were experimentally obseved in InAs (Fomin, 1984; Kornyushkin, 1996; Kurishev, 2001). The tunneling transitions of light holes were only considered because they have much greater tunneling probability compare to havy holes. It has been assumed that the electric field strength in the depletion region has maximum value. The correct choice of the electric field strength is important since it appears in the exponent of expressions (15-17). It must be pointed out that previously values of average and maximum electric field were used in theoretical calculations (Rosenfeld & Bahir, 1992; Kinch, 1981). The performed calculations showed that in homogeneous p^+-p_o-n_o–n junctions the band-to-band and trap-assisted tunneling currents are substantially less than the

measured current at reverse bias voltages U<1 V. The same result was obtained for asymmetrical p-n junctions in the case of the carrier concentartin is less than 10^{16} cm^{-3}. The reason of this result is that the electric field in the depletion region is too low to enable effective band-to-band and trap-assisted tunneling. To explain experimental results, models of a non-homogeneous p-n junction with non-uniform distribution of shallow and deep defects in the depletion region should be considered.

In such a junction the electric field and depletion region width are fluctuated. In a model of the band-to-band tunneling current proposed by Raikh and Ruzin (Raikh & Ruzin,1985; Raikh & Ruzin, 1987), the non-homogeneous distribution of impurities results in fluctuations of the depletion region width and, therefore, the tunneling distance for carriers. The electric conductivity of such a junction is mainly determined by small regions with high local concentration of impurities. Unfortunately, Raikh and Ruzin's model is valid at large reverse biase voltages $qU > E_g$ and can't be used for analysis of tunnell current in the investigated PDs at actual low voltages. Large deviation of impurity concentration in local regions of the junction results in increase in the electric field strength over the value typical for uniform distribution of charged defects. There are some arguments that these regions are related with Cottrell's atmospheres around dislocations (see below). So, it has been assumed that each region has the effective area of the order of 1 μm^2. Experimentally, atmospheres of impurity atoms around dislocations with similar dimensions were observed in GaAs (Bruk, 1982). The density of regions was assumed to be equal to the density of dislocation in the starting material. The electric field strength F served as an adjusting parameter in calculations. The relation between F and effective concentration of charged defects N is given by

$$F = \frac{qNW}{\varepsilon_s \varepsilon_o} \tag{21}$$

Shown in Fig.10 the trap-assisted tunneling current was calculated for the following carrier transition paths: traps are exchanged with both bands by thermal and tunnel transitions (curve 1), tunnel transitions of carriers from the valence band to traps followed by thermal and tunnel transitions to the conduction band (curve 2), tunnel transitions of carriers from the valence band to the conduction band (curve 3). The concentration of traps was varied in the range of 10^{13} - 10^{15} cm^{-3}. The best fit was obtained for concentrations of charged defects in the local regions of the order of 4×10^{16} cm^{-3}. This value is more than one order of magnitude higher than the mean concentration of free carriers obtained from the capacitance-voltage measurements. Obviously, the capacitance is determined by the homogeneous part of the junction, whereas the current flows mainly through the non-homogeneous regions. As seen, discrepancies between the calculated characteristics for different transition paths of carriers are not so significant to make an unambiguous choice. However, conclusion about the dominant contribution of the trap-assisted tunneling current at the reverse bias voltages U < 1 V seems to be apparent. At higher voltages both band-to-band and trap-assisted tunneling currents have comparable magnitude. The convergence of I-U curves in Fig.7 < which were measured at different temperatures, clearly indicates tunneling nature of the reverse current at large voltages U > 1 V. Despite the fact that the best fit was obtained for the trap-assisted tunneling current, additional investigations of tunneling mechanismsm are needed.

In order to clarify the role of the trap-assisted current in diffused PDS effect of ultrasonic treatment on the current-voltage characteristics was investigated (Sukach & Tetyorkin,

2009). Representative PDs were subjected to ultrasonic vibration with frequency 5-7 MHz and intensity ~0.4 W/cm² during 1 hour at room temperature. The second two-hour ultrasonic treatment with the same intensity was repeated after 72 hours. At last, experimental measurements were repeated afte nine-month storage of PDs at laboratory conditions.

Experimental data are shown in Fig. 11. Drastic increase in the measured forward current was revealed as a result of the second ultrasonic treatment. After nine-month storage the forward current is practically decreased to the starting values. It must be pointed out, that only the part of the current-voltage characteristic associated with the tunneling current is changed under ultrasonic treatment. Because of the pre-threshold intensity regime was used for ultrasonic treatment, experimental results can be explained by transformation of existing complex defects rather than generation of new point defects. Most probably that this transformation is connected with Cottrell's atmospheres around dislocations which intersect the p-n junction. In accordance with the vibrating string model of Granato-Luecke (Granato & Luecke, 1966), the intensive sonic-dislocation interaction results in an effective transformation of the absorbed ultrasonic energy into the internal vibration states of a semiconductor stimulating different defect reactions. The driving force of relaxation may be deformation and electric fields around dislocations.

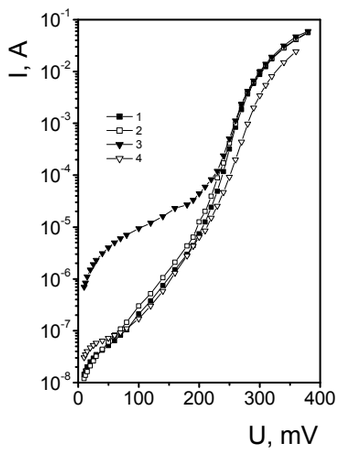

Fig. 11. Forward current vs voltage in a PD before (1) and after two sequential ultrasonic treatments (curves 2 and 3, respectively), and after nine-month storage (4), (Sukach & Tetyorkin, 2009).

The current-voltage characteristics of a representative heterojunction p^+-InAsSbP/n-InAs PD are shown in Fig. 12 and 13. The abrupt p-n junction formation in heterojunction PDs has been obtained from the barrier capacitance measurements. From the slope of C^{-2}-U characteristics the concentration of free carrirs in the range of $(2\div4)\times10^{16}$ cm^{-3} was determined. These values are in accordance with the electron concentration in the starting material. At two actual temperatures 290 K and 221 K the diffusion potential equals 0.2±0.01 V and 0.27±0.01 V, respectively.

Contrary to a diffused PD, the forward current in a heterojunction PD is characterized by one exponential dependence, Fig. 12. The ideality factor is changed from 1.1 at room temperature to 2.0 at 193 K. Thus, we can conclude that the bulk diffusion and recombination in the depletion region are dominant transport mechanisms at forward

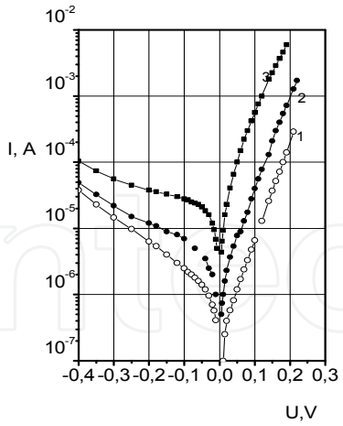

Fig. 12. Current-voltage characteristics of a representative heterojunction PD at temperatures, K: 193 (1), 228 (2) and 290 (3) (Tetyorkin, 2005).

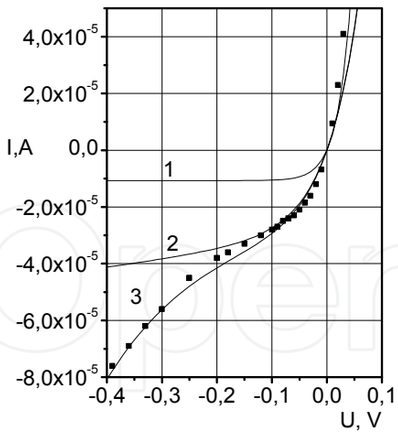

Fig. 13. Measured (dots) and calculated (lines) currents in a heterojunction PD at 295 K. Calculated curves represent diffusion (1), generation-recombination (2) and trap-assisted tunneling (3) mechanisms. The fit was obtained for $N_t = 6\times10^{13}$ cm^{-3}, n = 4×10^{16} cm^{-3}, $E_t = E_g/2$, $\tau_o = 6\times10^{-8}$ s, $\mu_p = 150$ cm^2/V×s. (Tetyorkin, 2005).

biases. At the same time, the reverse current was not saturated even at room temperature. As seen from Fig. 13, it has a form typical for the soft breakdown. The fitting calculation of the reverse current proved primary contribution of generation and trap-assisted tunneling currents at applied reverse bias voltages. The trap-assisted tunneling current was calculated for the following carrier transitions: traps are exchanged carriers with the valence band by thermal and tunnel transition, and with the conduction band by tunnel transitions only. Despite the fact that the fit was achieved for resonable values of trap concentration and energy, additional investigations are needed to clerify mechanisms of tunneling. In particular, the role played by the dislocation network at the InAs-InAsSbP heterojunction must be thoroughly investigated. At the reverse biase voltages U > 1.0 V the band-to-band tunneling seems to be dominant.

5. Performance of InAs photodiodes

5.1 Current sensitivity

The current sensitivity of PDs is given by

$$S_i = \frac{e}{hc}\eta\lambda = \frac{e}{hc}\lambda(1-R)\beta[1-\exp(-kd)]\alpha_{p-n} \quad (22)$$

where η is the quantum efficiency, β is the quantum yield of the internal photoeffect, d is the width of the photodiode's structure, and $\alpha_{p\text{-}n}$ is the collecting coefficient (G.S Oliynuk, 2004). It is known that three regions in the p-n junction can contribute to the photocurrent, namely: two quasineutral regions of p- and n-type conductivity and the depletion region. The excess carriers excited in these regions can be collected by the junction. In the diffused PDs the

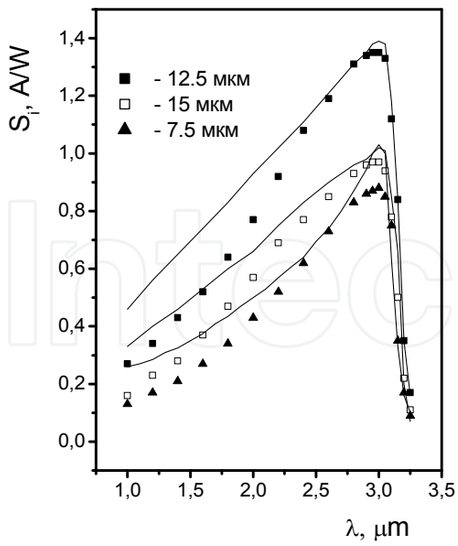

Fig. 14. Calculated (solid lines) and measured (dots) spectral dependences of current sensitivity in diffused PDs with different junction depth at 77 K and concentration of carriers in the compensated region, cm^{-3} : $8\ 10^{15}$ (▲), $5\ 10^{15}$ (□) and $2\ 10^{15}$ (■).

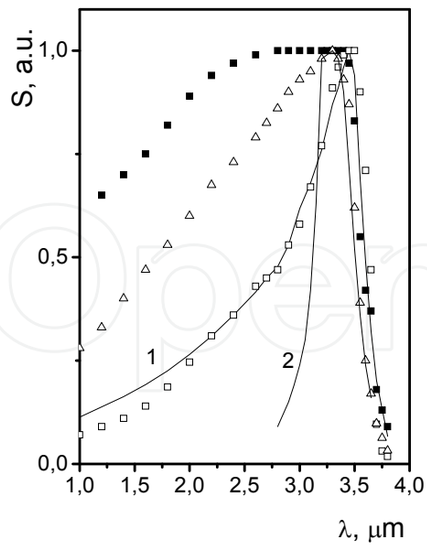

Fig. 15. Spectral dependences of sensitivity in homojunction (open dots and triangles) and heterojunction (close dots) PDs at 295 K (Tetyorkin, 2007). The junction depth in homojunction PDs equals 8 (□) and 4 (Δ) μm, respectively. Also shown is the emission spectrum of InAs LED (2).

current sensitivity $S_i(\lambda)$ is found to be basically determined by the quasineutral p-type region. The quasineutral n-type region contributes mainly to the long wavelength photosensitivity. The contribution of the depletion region is negligibly small in the whole spectral region (G.S Oliynuk, 2004). As seen from Fig. 14, the current sensitivity in the diffused PDs is not less than in commercially available InAs photodiodes.

The broadband spectrum shown in Fig. 15 is explained by contribution of both sides of the heterojunction PD, including heavily doped wide-gap InAsSbP constituent, to the photoresponse (Tetyorkin, 2007). The spectral dependence of photosensitivity in heterojunction PD is superior to homojunction one due to effect of "wide-gap window".

5.1 Resistance-area product

The differential resistance-area product at zero bias R_0A determines threshold parameters of infrared PDs. Theoretical limitations of threshold parameters in InAs PDs are related to the fundamental (radiative and Auger) recombination processes. The SRH recombination is considered as nonfundemental since it can be reduced by improvement in technology of PDs.

In the diffusion-limited asymmetrical p^+-n junction the product R_0A is given by

$$(R_oA)_D = \frac{(kT)^{1/2}}{q^{3/2}} \frac{n_o}{n_i^2} \left(\frac{\tau_p}{\mu_p}\right)^{1/2} \tag{23}$$

In the case of generation-recombination current it can be expressed as

$$(R_oA)_{GR} = \frac{4(kT/q)}{qn_iW/\tau_0} \quad (24)$$

The last formula is obtained by differentiating the well known expression $I=I_o[\exp(eU/2kT)1]$, where $I_o=qn_iW/2\tau_o$. Since experimental data were obtained at zero and small forward voltages (<10 mV) the depleted region width W was assumed to be independent on U.

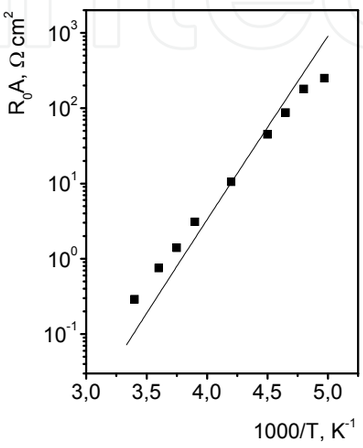

Fig. 16. Experimental (dots) and calculated (solid line) data dependences of R_oA vs. temperature in symmetrical p-n junction ($p=n=3\times10^{15}$ cm^{-3}) for diffusion mechanism of carrier transport. (Tetyorkin, 2007)

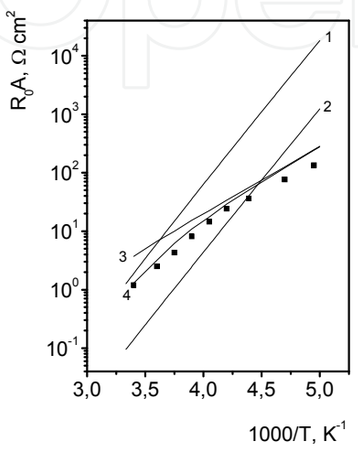

Fig. 17. Experimental (dots) and calculated (solid lines) dependences of R_oA vs. temperature in InAs p^+-n (1) and n^+-p (2) junctions. Calculated dependences were obtained for diffusion current (1,2) and recombination current in the depletion region (3). The doping level is equal to 3×10^{16} (1) and 5×10^{16} (2) cm^{-3}. Also shown is the R_0A product for diffusion and generation-recombination current in p^+-n junction with $n=3\times10^{16}$ cm^{-3} (4). Experimental data are measured in a p^+-n heterojunction PD with $n=3\times10^{16}$ cm^{-3} (Tetyorkin, 2007)

The measured and calculated values of R_oA in symmetrical homojunctin and asymmetrical heterojunction PDs are shown in Fig.16 and 17. The electron and hole mobility used in the calculation were approximated by the dependence $\mu(T)= \mu_0(T/300)^{-0.5}$, where μ_0 is the mobility at T=300 K. The effective lifetime was assumed to be determined by radiative and Auger 1 (Gelmont) recombination mechanisms. Since the electron mobility in InAs exceeds the hole mobility by approximately two orders of magnitude, the diffusion-limited PDs of p^+-n type can potentially have the highest values of R_oA, Fig.17. The calculated values of the current sensitivity S_i, differential-resistance product R_0A and specific detectivity are summarized in Table. The current sensitivity and detectivity was calculated for the peak wavelength λ_p. It should be pointed out that typical values of the specific detectivity in the investigated heterojunction PDs are of the order of $2\cdot10^9$ cm×Hz$^{1/2}$×W^{-1}. Approximately the

same values of detectivity were obtained in commercially available PDs. However, at room temperature the resistance-area

Parameters of InAs photodiodes						
T_0, °C	A, см$^{-2}$	λ_p, μm	$S_i(\lambda_p)$, A/W	R_0A, Ωcm^{-2}	D_λ^*, cm·Hz$^{1/2}$W^{-1}	Manufacturer
22	$7.86\cdot10^{-3}$	3.35	1.0	0.12 - 0.20	$2.7\cdot10^{9}$	Judson
-85	$7.85\cdot10^{-3}$	3.20	1.5	196 – 393	$3.6\cdot10^{11}$	Judson
25	$7.85\cdot10^{-3}$	3.35	1.0	0.31 – 0.55	$(3.0 – 4.5)\cdot10^{9}$	Hamamatsu
-196	$7.85\cdot10^{-3}$	3.00	1.3	$(0.8 – 8.0)\cdot10^{3}$	$(3.5 – 6.0)\cdot10^{11}$	Hamamatsu
20	$1.45\ 10^{-3}$	2.60-3.40	0.7-0.8	1.5-2.0	$(2.5\text{-}3.0)\ 10^{9}$	IOFFE PTI, St.-Petersburg
25	$1.0\cdot10^{-2}$	3.45 – 3,50	0.8	0.15 – 0.30	$2.0\cdot10^{9}$	ISP, Kiev
-196	$1.0\cdot10^{-2}$	3.00	1.2 – 1.3	$(0.5 – 2.0)\cdot10^{5}$	$(5.0 – 6.0)\cdot10^{11}$	ISP, Kiev
-196	$1.0\ 10^{-2}$	3.00	2.4	$1\ 10^{11}$	$2\ 10^{12}$ (BLIP)	ultimate parameters

product in the heterojunction PDs is five times higher. Taking into account their broadband spectral response, one can conclude that the heterojunction PDs can be more effective as sensitive element in gas sensors operated at room and near-room temperatures. The ultimate parameters shown in Table were calculated for the generation-recombination limited p^+-p_o-n_o-n junction with $n_o=p_o= 3\ 10^{15}$ cm^{-3}. The current sensitivity and specific detectivity were calculated using the formulas (22) and (24) for the experimentally measured parameters W=0.63 μm and $\tau_o = 8\ 10^{-8}$ s. It is assumed that the quantum efficiency was equal to 1.0. At 77 K the intrinsic concentration in InAs is $2.1\ 10^3$ cm^{-3}. Parameters of PDs produced by Judson and Hamamatsu were taken from their web sites. As seen, in the generation-recombination limited PDs BLIP mode of operation can be realized.

6. New trends in development of InAs-based infrared detectors

InAs PDs are usually fabricated from bulk single crystall wafers. The p-n junctions are formed by ion (e.g. Be) implantation or Cd diffusion. Obviously, further progress in development of InAs infrared detectors including multielenment structures is closely connected with technology of epitaxial films. Diffetent epitaxial techniques including liquid-phase epitaxy (LPE), gas-phase epitaxy (GPE) and moleqular-beam epitaxy (MBE) were used in different laboratories for growth of InAs-based epitaxial films. Currently, their quality has not reached the level of maturity required for manufacture of electronically scanned multielement structures. As a rule, the as-grown LPE films has a high concentration of residual impurities which affect the lifetime and mobility of carriers. The low concentration of residual impurities in epitaxial layers is a crucial condition for improvement in performance of InAs-based infrared detectors. Effect of gadolinium doping on quality of InAsSbP epitaxial films was demostrated (Matveev, 2002). It is known that the rare earth impuruty doping results in a gettering effect in semiconductors. Epitaxial films grown by LPE technique from the melt doped with gadolinim exhibited better photoluminescence efficiency and higher mobility of carriers. As a result, the diffusion-limited InAs/InAsSbP heterosructure PDs with improved characteristics were manufactured (Matveev, 2002).

InAs PDs were also grown by molecular beam epitaxy (MBE) on alternative GaAs and GaAs-coated silicon substrates (Dobbelaere, 1992). The relatively high doping level (>10^{16} cm^{-3}) in the active region was used for the junction formation. The PDs were diffusion-limited at temeperatures as low as 160 K. At 77 K the dominant current is expected to be the defect-assisted tunneling current. Also, in these PDs rather high detectivity of the order of 7 10^{11} cm $Hz^{1/2}W^{-1}$ was achieved at the peak wavelength 2.95 μm. In opinion of the authors these results clearly demostrate the feasibility of the monolithic integration of InAs infrared detectors and GaAs or Si read-out electronics.

The cut-off wavelength in InAs PDs is 3-4 μm whicn is not enough to cover the atmospheric windows 3-5 entire μm. Therefore, ternary compounds InAsSb with more narrow bang gap were extensively investigated as a material for infrared detectors with longer cut-off wavelength. InAsSb epitaxial films were grown on GaAs substrates by MBE in IMEC, Belgium (Merken, 2000). Linear and two-dimensional focal-plane arrays with 256x256 pixels were realized. At room temperature the product R_oA was limited by the combined generation-recombination and diffusion currents.

Multielement InAs MOS capacitors were developed in A.V. Rzhanov Institute of Semiconductor Physics, Russia (Kuryshev, 2009). Auotoepitaxial films were grown on n-InAs substrates. The films were characterized by the electron concentration (1-5) $\cdot 10^{15}$ cm^{-3} and the carrier lifetime 0.3-1.8 μs at 77 K. The SiO_2 gate oxide with thickness of the order of 130 nm was deposited on a previously grown 15 nm thick anode oxide doped with fluorine. The surface states density of the order of to 2 $\cdot 10^{10}$ cm^{-2} eV^{-1} was obtained compare to 3 $\cdot 10^{11}$ cm^{-2} eV^{-1} in undoped films. Linear (1x384) and two-dimensional (128x128, 256x256) focal-plane arrays have been made. The specific detectivity in typical 128x128 assembly with pixel size 40x40 μm was 3 $\cdot 10^{12}$ cm $Hz^{1/2}W^{-1}$ (λ=2.95 μm) at 80 K. Infrared devices (thermal imaging camera, microscope and spectrograf) with improved characteristics were designed.

A new type PDs based on InAs/GaSb superlattices have been recently developed in several laboratories (Rehm, 2006). They were grown by MBE on GaSb substrates. The PDs have p-i-n structure with the type-II short-period superlattice intrinsic region embedded between highly doped contact layers. The superlattice material has some advantages over bulk InAs. The band gap of the superlattice can be varied in a range between 0 and about 250 meV. The Auger recombination can be significantly suppressed, since electrons and holes are spatially separated in neighboring layers. In the single-element test diodes with the cut-off wavelength 5.4 μm at 77 K values of R_oA= 4 $\cdot 10^5$ Ω $\cdot cm^2$ were measured. The diodes were limited by generation-recombination currents and show background limited performance. The quantum efficience as high as 60% and current responsivity of 1.5 A/W were achieved. High-performance 256x256 focal plane arrays on InAs/GaSb superlattice PDs were manufactured designed for 3-5 μm and 8-12 μm spectral regions (Rehm, 2006; Hill, 2008). Excellent thermal images with noise equivavlent temperature difference below 10 mK were realized. Despite these advantages, several problems such as the surface leakage current, band-to-band and trap-assisted tunneling currents should be solved for improving the superlattice PDs performance.

7. Conclusions

1. The carrier lifetime is investigated in *n*- and *p*-type InAs as a function of carrier concentration and temperature. It is proved that experimental data can be correctly explained by radiative recombination mechanism in both *n*- and *p*-type InAs at

temperatures close to 77 K. The lifetime in *p*-InAs is determined by three recombination mechanisms - radiative, Auger 7 and Auger S. The role of the Auger S recombination in p-InAs seems to be overestimated in the developed theoretical models. The contribution of the Shockley-Read-Hall recombination should be clarified. It is shown that the developed models of recombination can correctly predict the most important parameters of InAs-based infrared PDs.

2. The diffused homojunction PDs have threshold parameters comparable with commercially available ones. It is proved that p^+-InAsSbP/*n*-InAs heterojunction PDs may be more suitable for application in gas sensors which are operated at room temperature. The threshold parameters in conventional PDs may be improved by supression of the Auger recombination and reduction of the trap-assisted tunneling current.
3. Furter progress in manufacture of conventional single-element PDs is most likely associated with epitaxial films grown on InAs or alternative substrates. Linear and two-dimensional photodiode arrays based on InAs bulk technology which can be attributed to the second generation infrared detectors are in the early stage of development.
4. The results achived in InAs/GaSb type-II superlattice PDs confirm that InAs-based technology is now competitive for manufacture infrared devices with high performance.

8. References

Andrushko, A.I.; Selihov, A.I., Slobodchikov, S.V. (1986). On the recombination mechanism in indium arsenide crystals, *Fiz. Tekh. Poluprov.* (In Russia), Vol. 20, N3, 403-406, ISSN 0015-3222.

Barishev, N.S. (1964). Band-to-band recombination of electrons and holes in indium arsenide, *Fiz. Tverdogo Tela* (In Russia), Vol. 5, N10, 3027-3030, ISSN 0367-3294.

Beattie, A.R. (1962). Quantum Efficiency in InSb, *J.Phys.Chem.Solids*, Vol. 23, 1049-1056, ISSN 0022-3697.

Beattie, A. & Landsberg, P.T. (1959). Auger effect in semiconductors, *Proc. Roy. Soc. A.*, Vol. 249, 16-29, ISSN 0308-2105.

Beattie A.R & Smith G. (1967). *Phys. status solidi*, Vol.19, N3, 577-586, ISSN 0031-8965.

Blakemore J.S. (1962). *Semiconductor Statistics*, Pergamon Press, Oxford, ISBN 0486495027.

Blaut-Blachev, A.N.; Balagurov, L.A., Karatayev, V.V. et. al. (1975). Carrier recombination in n-InAs, *Fiz. Tekh. Poluprov.* (In Russia), Vol. 9, N4, 782-784, ISSN 0015-3222.

Bolgov, S.S., Malyutenko, V.K, Savchenko A.P. (1997). Exclusion of carriers in InAs, *Fiz. Tekh. Poluprov.* (In Russia), Vol. 31, N5, 526-527, ISSN 0015-3222.

Bruk, A.S.; Govorkov, L.I., Kolesnik , L.I. (1982). The role of interaction dislocation-point defect-dopant in the recombination processe in gallium arsenide, *Fiz. Tekh. Poluprov.* (In Russia), Vol. 16, N8, 1510-1512, ISSN 0015-3222.

Datal, V.L.; Hicinbothem, W.A. & Kressel, H. (1979). Carrier lifetimes in epitaxial InAs, *Appl. Phys. Lett.*, Vol. 24, 184-185, ISSN 0003-6951.

Dobbelaere W.; De Boeck G., Heremans P., Mertens R., and Borghs G. (1992). InAs p-n diodes grown on GaAs and GaAs-coated Si by molecular beam epitaxy, *Appl. Phys. Lett.*, Vol. 60, N7, 868-870, ISSN 0003-6951.

Fomin, I.A.; Lebedeva, L.V., Annenko, N.M. (1984). Investigation of deep defect levels in InAs by capacitance measurements of MIS structures, *Fiz. Tekh. Poluprov.* (In Russia), Vol. 18, N3, 734-736, ISSN 0015-3222.

Gelmont, B.L. (1978). Three-Band Kane Model of Auger Recombination, *Zh. Eksper. Teor. Fiz.* (In Russia), Vol. 75, N2, 536-544, ISSN 0044-4510.

Gelmont, B.L. (1981). Auger Recombination in Narrow-Gap p-Type Semiconductor, *Fiz. Tekh. Poluprov.* (In Russia), Vol. 15, N7, 1316-1319, ISSN 0015-3222.

Gelmont, B.L.; Sokolova, Z.N. & Yassievich, I.N. (1982). Auger Recombination in Direct-Gap p-Type Semiconductors, *Fiz. Tekh. Poluprov.* (In Russia), Vol. 16, N3, 592-600, ISSN 0015-3222.

Gelmont, B.L. & Sokolova, Z.N. (1982). Auger Recombination in Direct-Gap n-Type Semiconductors, *Fiz. Tekh. Poluprov.* (In Russia), Vol. 16, N9, 1670-1672, ISSN 0015-3222.

Granato A.V. & Luecke K. (1966), in *Physical Acoustic*, ed. W.P. Mason, Academic Press, New York, ISBN 0387984356.

Grigor'ev, N.N. & Kudykina, T.A. (1997). Recombination model of Zn diffusion in GaAs, *Fiz. Tekh. Poluprov.* (In Russia), Vol. 31, N6, 697-702, ISSN 0015-3222.

Kinch M.A. (1981). Metal-insulator semiconductor infrared detectors. In *Semiconductor and Semimetals*, vol. 18, R.K. Willardson and A.C. Beer, Eds., New York: Academic Press, 1981, ch.7.

Kornyushkin, N.A.; Valisheva N.A., Kovchavtsev A.P., Kuryshev G.L. (1996) Effect of interface and deep levels in the gap on capacitance-voltage characteristics of GaAs MIS structures, *Fiz. Tekh. Poluprov.* (In Russia), Vol. 30, N5, 914-917, ISSN 0015-3222.

Kuryshev G.L.; Kovchavtsev A.P., Valisheva N.A. (2001), Electronic properties of metal-insulator-semiconductor structures, *Fiz. Tekh. Poluprov.* (In Russia), Vol. 35, N9, 1111-1119, ISSN 0015-3222.

Kuryshev G.L.; Lee I.I., Bazovkin V.M. et al. (2009). Ultimate parameters of multielement hybrid MIS InAs IR FPA and devises based of them, *Prikladnaya Fizika* (In Russia), N2, 79-93, ISSN 1996-0948.

Madelung, O. (1964). *Physics of III-V semiconductors*. New York-London-Sydney.

Matveev, B.A.; Gavrilov, G.A., Evstropov, V.V. et. al. (1997). Mid-infrared (3-5 μm) LEDs as sources for gas and liquid sensors, *Sens. Actuators B*, Vol. 38-39, 339-343, ISSN 0925-4005.

Matveev, B.A.; Zotova, N.V., Il'inskaya, N.D. et al. (2002). Towards efficient mid-IR LED operation: optical pumping, extraction or injection of carriers?, *J. Mod. Opt.*, Vol. 49, N5/6, 743-756, ISSN 0950-0340.

Merken P.; Zimmermann L., John J., Nemeth S., Gastal M., Van Hoof C. (2000). InAsSb and InGaAs linear and focal-plane arrays, *Proc. SPIE*, Vol.4028, 246-251, ISSN 0277-786X.

Nemirovsky, Y. & Unikovsky, A. (1992). Tunneling and 1/f noise currents in HgCdTe photodiodes, *J. Vac. Sci. Technol. B*, Vol. 10, N4, 1602-1610, ISSN 0022-5355.

Oliynuk G.S, Sukach A.V., Tetyorkin V.V, Stariy S.V, Lukyanenko V.I, Voroschenko A.T. (2004), Uncooled InAs photodiodes for optoelectronic sensors, *Proc. SPIE,* Vol.5564, 143-148, ISSN 0277-786X.

Popov, F.A.; Stepanov, M.V., Sherstnev, V.V. & Yakovlev, Yu.P. (1997). 3.3 μm LEDs for measurements of methane, *Tech. Phys. Lett.*, Vol. 23, 24-31, ISSN 1063-7850.

Raikh, M.E. & Ruzin I.M. (1985). Fluctuation mechanism of excess tunneling currents in reverse biased p-n junctions", *Fiz. Tekh. Poluprov.* (In Russia), Vol. 19, N7, 1216-1225, ISSN 0015-3222.

Raikh, M.E. & Ruzin I.M. (1987). Temperature dependence of excess fluctuation currents through meta-semiconductor contact, *Fiz. Tekh. Poluprov.* (In Russia), Vol. 21, N3, 456-460, ISSN 0015-3222.

Rogalski, A. & Orman, Z. (1985). Band-to-band recombination in $InAs_{1-x}Sb_x$, *Infrared Phys.*, Vol. 25, N3, 551-560, ISSN 0020-0891.

Rogalski, A. (ed.) (1995). Infrared Photon Detectors, *SPIE Optical Engineering Press*, ISBN, 0 8194 1798 X, N.Y.

Rosenfeld D. & Bahir G. (1992). A model for the trap-assisted tunnelling mechanism in diffused n-p and implanted n^+-p HgCdTe photodiodes, *IEEE Trans. On Electron Devices*, Vol. 39, N7, 1638-1645, ISSN 0018-9383.

Sukach A., Tetyorkin V., Olijnyk G, Lukyanenko V., Voroschenko A. (2005), Cooled InAs photodiodes for IR applications, *Proc. SPIE.*, Vol.5957, 267-276, ISSN 0277-786X.

Sukach A.V.& Tetyorkin V.V. (2009) Ultrasonic treatment-induced modification of the electrical properties of InAs p-n junctions, *Tech. Phys. Lett.*, Vol.36, N6, 514-517, ISSN 1063-7850.

Sze, S.M. (1981). *Physics of Semiconductor Devices*, second edition, Wiley, N.Y. ISBN 0471056618.

Takeshima, M. (1972). Auger Recombination in InAs, GaSb, InP and GaAs, *J. Appl. Phys.*, Vol. 43, N10, 4114- 4119, ISSN 0021-8979.

Takeshima M. (1975). Effect of electron-hole interaction on the Auger recombination process in a semiconductor, *J. Appl. Phys.*, V. 46, N7, 3082-3088, ISSN 0021-8979.

Tetyorkin V. V., Sukach A. V., Stariy S. V., Zotova N. V., Karandashev S. A., Matveev B. A., Stus N. M. (2005). p+-InAsSbP/n-InAs photodiodes for IR optoelectronic sensors, *Proc. SPIE*, Vol.5957, 212-219 ISSN 0277-786X.

Tetyorkin V.V., Sukach A.V., Stary S.V., Zotova N.V., Karandashev S.A., Matveev B.A., Remennyi M.A.,Stus N.M. (2007), Performance of InAs-based Infrared Photodiodes, *Proc. SPIE.,* Vol. 6585, 185-194, ISSN 0277-786X.

Van Roosbroeck W. & Shockley W. (1954). Photon-radiative recombination of electrons and holes in germanium, *Phys. Rev.*, Vol. 94, 1558-1560, ISSN 1098-0121.

Wenmu He, Zeynep Celik-Batler. (1996). 1/f noise and dark current components in HgCdTe MIS infrared detectors, *Solid-State Electron,* Vol. 19, N1, 127-132, ISSN 0038-1101.

Wider, H.H. & Collins, D.A. (1974). Minority carrier lifetime in InAs epilayers, *Appl. Phys. Lett.*, Vol. 25, 742-743, ISSN 0003-6951.

Zotova, N.V.; Karandashev, S.A., Matveev, B.A. et. al. (1991). Optoelectronic sensors based on narrow band A^3B^5 alloys, *Proc. SPIE*, Vol. 1587, 334-345, ISSN 0277-786X.

Rehm, R; Walther M., Schmitz J. Et al. (2006). InAs/GaSb superlattice focal plane arrays for high-resolution thermal imaging, *Opto-Electronics Review*, Vol.14, N1, 19-24, ISSN 1230-3402.

Hill, C. J.; Soibel, A., Keo, S.A., et al (2008). Infrared imaging arrays based on superllatice photodiodes, *Proc. SPIE*, Vol. 6940, 69400C-1 – 69400C-10, ISSN 0277-786X.

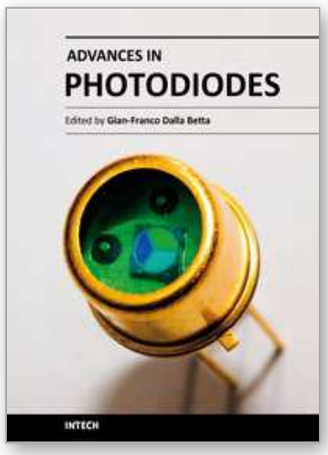

Advances in Photodiodes

Edited by Prof. Gian Franco Dalla Betta

ISBN 978-953-307-163-3
Hard cover, 466 pages
Publisher InTech
Published online 22, March, 2011
Published in print edition March, 2011

Photodiodes, the simplest but most versatile optoelectronic devices, are currently used in a variety of applications, including vision systems, optical interconnects, optical storage systems, photometry, particle physics, medical imaging, etc. Advances in Photodiodes addresses the state-of-the-art, latest developments and new trends in the field, covering theoretical aspects, design and simulation issues, processing techniques, experimental results, and applications. Written by internationally renowned experts, with contributions from universities, research institutes and industries, the book is a valuable reference tool for students, scientists, engineers, and researchers.

How to reference

In order to correctly reference this scholarly work, feel free to copy and paste the following:

Volodymyr Tetyorkin, Andriy Sukach and Andriy Tkachuk (2011). InAs Infrared Photodiodes, Advances in Photodiodes, Prof. Gian Franco Dalla Betta (Ed.), ISBN: 978-953-307-163-3, InTech, Available from: http://www.intechopen.com/books/advances-in-photodiodes/inas-infrared-photodiodes

INTECH
open science | open minds

InTech Europe
University Campus STeP Ri
Slavka Krautzeka 83/A
51000 Rijeka, Croatia
Phone: +385 (51) 770 447
Fax: +385 (51) 686 166
www.intechopen.com

InTech China
Unit 405, Office Block, Hotel Equatorial Shanghai
No.65, Yan An Road (West), Shanghai, 200040, China
中国上海市延安西路65号上海国际贵都大饭店办公楼405单元
Phone: +86-21-62489820
Fax: +86-21-62489821

IntechOpen